

## Article

# Orthorhombic Crystal Structure of Grossular Garnet (Suva Česma, Western Serbia): Evidence from the Rietveld Refinement

Pavle Tančić <sup>1,\*</sup> , Slađana Dušanić <sup>2</sup> and Suzana Erić <sup>3</sup>

<sup>1</sup> Department for Catalysis and Chemical Engineering, Institute of Chemistry, Technology and Metallurgy, University of Belgrade, Njegoševa 12, 11000 Belgrade, Serbia

<sup>2</sup> Geological Survey of Serbia, Rovinjska 12, 11000 Belgrade, Serbia; dusanics71@gmail.com

<sup>3</sup> Faculty of Mining and Geology, University of Belgrade, Djušina 7, 11000 Belgrade, Serbia; suzana.eric@rgf.bg.ac.rs

\* Correspondence: pavletan@gmail.com

**Abstract:** The grossular garnet from rodingite-type rock from the Suva Česma area in western Serbia is characterized with its weak anisotropic nature. Because its anisotropy could indicate a non-cubic lower symmetry, SEM-EDS and Rietveld powder refinement methods were used. The SEM-EDS results have shown that the garnet has a  $(\text{Ca}_{3.00}\text{Mn}_{0.01})_{3.01}(\text{Al}_{1.82}\text{Fe}_{0.15}\text{Ti}_{0.02})_{1.99}(\text{Si}_{2.97}\text{Al}_{0.03})_{3.00}\text{O}_{12}$  chemical composition (i.e.,  $\text{Grs}_{91}\text{Adr}_{08}$ ), which can be more specifically explained as ferric iron containing grossular. The next step further used Rietveld powder refinements of the various crystal structures in the  $Ia\bar{3}d$ ,  $R\bar{3}c$ ,  $R\bar{3}$ ,  $I4_1/a$ ,  $Fddd$ ,  $C2/c$ , and  $I\bar{1}$  space groups as well as a single mixture, which was followed by a comparative analysis of the  $R$ -values, site occupancy factors, and bond lengths and angles. The synthesis of these results showed both that the studied grossular garnet is not cubic and that it crystallized in the disordered  $Fddd$  space group with the final  $R_B = 5.29\%$  and  $R_F = 1.75\%$ . It was presumed that the grossular formed at temperatures between 150 and  $\sim 600$  °C.

**Keywords:** grossular garnet; rodingite; Suva Česma (western Serbia); Rietveld powder refinement method; orthorhombic crystal structure; disordered  $Fddd$  space group



check for updates

**Citation:** Tančić, P.; Dušanić, S.; Erić, S. Orthorhombic Crystal Structure of Grossular Garnet (Suva Česma, Western Serbia): Evidence from the Rietveld Refinement. *Powders* **2023**, *2*, 387–402. <https://doi.org/10.3390/powders2020023>

Academic Editor: Paul F. Luckham

Received: 24 February 2023

Revised: 11 May 2023

Accepted: 16 May 2023

Published: 18 May 2023



**Copyright:** © 2023 by the authors. Licensee MDPI, Basel, Switzerland. This article is an open access article distributed under the terms and conditions of the Creative Commons Attribution (CC BY) license (<https://creativecommons.org/licenses/by/4.0/>).

## 1. Introduction

Field geological mapping and accompanied laboratory studies were conducted in the vicinity of Valjevo in Western Serbia to create a basic geological map. During this process, samples of Jurassic age ophiolites, such as serpentinites, gabbros, peridotites, andesites, diabases, and amphibolites, were mapped [1]. At the Suva Česma locality within the field exploration area, a single rock was detected that was rather unusual (Figure 1). This unknown rock was collected from contact with serpentinite; after using an optical microscopic, X-ray powder diffraction (XRPD), and chemical methods to determine its constraints, the rock was found to be rodingite [2].

The occurrence of rodingite at Suva Česma was the first example of this type of rock discovered in Serbia. The initial mineralogical constraints show that the Suva Česma rodingite can be characterized by its massive structure and granoblastic texture. The results further show that the rodingite primarily consists of macroscopically white, microscopically transparent, and weakly anisotropic grossular (i.e., >80%). Grossular appears in a coarse-grain granular form, with a size of ca. 0.5–1.5 mm. The calculated unit-cell, found through the XRPD method, indicated that this grossular has  $\text{Grs}_{98}\text{Adr}_2$  composition (the mineral abbreviations Grs and Adr refer to grossular and andradite, respectively [3]).



Green Mg-Al-Fe chlorite (Chl; [3]) occupies interstitials between the grossular grains in this rock. Pseudomorphic forms of chlorite, up to ca. 0.5 mm in size, are most likely to represent a secondary phase created by the alteration of pyroxene [2].

The typical mineral appearances of Grs and Chl as observed by the transmitted light microscopy are presented in Figure 2. Microscopic examination shows that grossular does not have visible twinning, zonation areas, or isotropic areas.

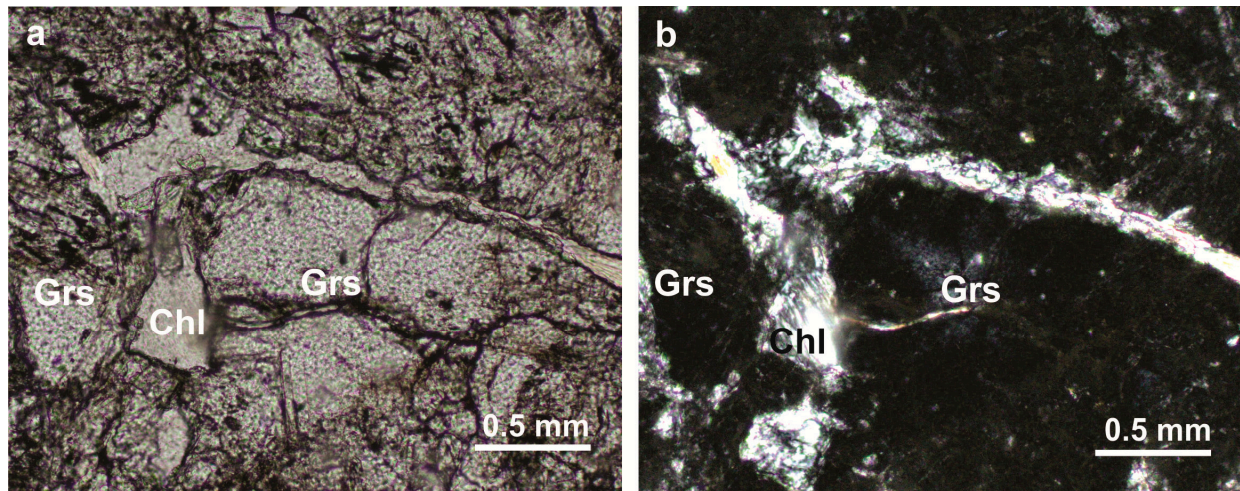


**Figure 2.** Typical mineral appearances of grossular (Grs) and chlorite (Chl) observed by the transmitted light microscopy: (a) parallel nicols; (b) crossed nicols.

In the following study, the main goal was to conduct an XRPD examination of the crystal structure of grossular garnet from the rodingite-type rock [2] using the Rietveld powder refinement method for several reasons, including:

1. Only three optically anisotropic grossular-andradite garnets from Serbia have been characterized so far (i.e., from skarns found in the Kopaonik Mts. [4–6], Rogozna Mts. [7], and Rudnik Mts. [8]);
2. We believe that the weak garnet anisotropy could indicate the presence of disymmetrization; there are five possible causes of this, discussed in [4–6]. In summary, it is agreed that the that grossular-andradite garnet group could exhibit non-cubic symmetry in various space groups (hereinafter, s.g.'s), such as:  $I\bar{1}$  [9–14];  $Fddd$  [9,12,15,16];  $Fddd$  or  $C2/c$  [17];  $R\bar{3}c$  or  $Fddd$  [5]; and  $R\bar{3}c$  [6]. More recently, it was shown that these minerals could have a tetragonal symmetry (most likely  $I4_1/a$  s.g.), as well [18].

To present a more reliable chemical composition of grossular garnet, we also used the results of the SEM-EDS investigations.

## 2. Materials and Methods

### 2.1. SEM-EDS Method

The SEM-EDS investigations were carried out at the University of Belgrade, Faculty of Mining and Geology, using a JEOL JSM-6610LV (JEOL Ltd., Tokyo, Japan) Scanning Electron Microscope (SEM; with a W-filament as a beam source), coupled with an XMax Energy Dispersive Spectrometer (EDS). The polished rodingite samples were coated with carbon using a BALTEC-SCD-005 sputter coating device. The results were recorded under high vacuum conditions with acceleration voltage of 20 kV. The following external standards were used to obtain garnet chemical compositions: almandine for Al, Si and Fe; spessartine for Mn; diopside for Ca; and  $TiO_2$  for Ti. Processing option was oxygen by stoichiometry, whereas the number of ions calculation was based on 8.00 cations per formula unit (hereinafter *apfu*).

## 2.2. XRPD Method

One selected rodingite sample was manually powdered and homogenized under alcohol in an agate mortar for several hours to ensure good statistical distribution of the grains. After that, it was placed in a bottom-loaded aluminum carrier. Diffraction data were collected at the University of Belgrade, Faculty of Mining and Geology, on a Phillips PW1710 diffractometer (PANalytical, Almelo, The Netherlands) equipped with a graphite monochromator (Cu  $K\alpha_1$ ,  $\lambda = 1.540562 \text{ \AA}$ ; Cu  $K\alpha_2$ ,  $\lambda = 1.544390 \text{ \AA}$ ) and an Xe-filled proportional counter; tests were conducted at room temperature (23 °C). Divergence and receiving slits were fixed to 1° and 0.1 mm, respectively. The generator was set up at 40 kV and 30 mA. The diffractometer alignment was checked using a reference material of powdered crystalline silicon according to the manufacturer's user manual. Data were collected in scan-step mode, with a 0.02° 2 $\theta$  step and between 4° and 135° 2 $\theta$  and 12.9s step<sup>-1</sup> for collecting data used for Rietveld structure refinements.

The procedure applied included Rietveld refinements of the crystal structures in a series of seven space groups and one mixture, followed by the comparative analysis of the *R*-values, site occupancy factors (hereinafter *sof*'s), and bond lengths and angles. Beyond these, the estimated standard deviations (hereinafter *esd*'s) were also considered as an additional accessory tool.

## 3. Results and Discussion

### 3.1. SEM-EDS Study

The SEM and BSE microphotographs of Grs and Chl are presented at Figure 3 and show that there is no visible twinning or zonation in the grossular.

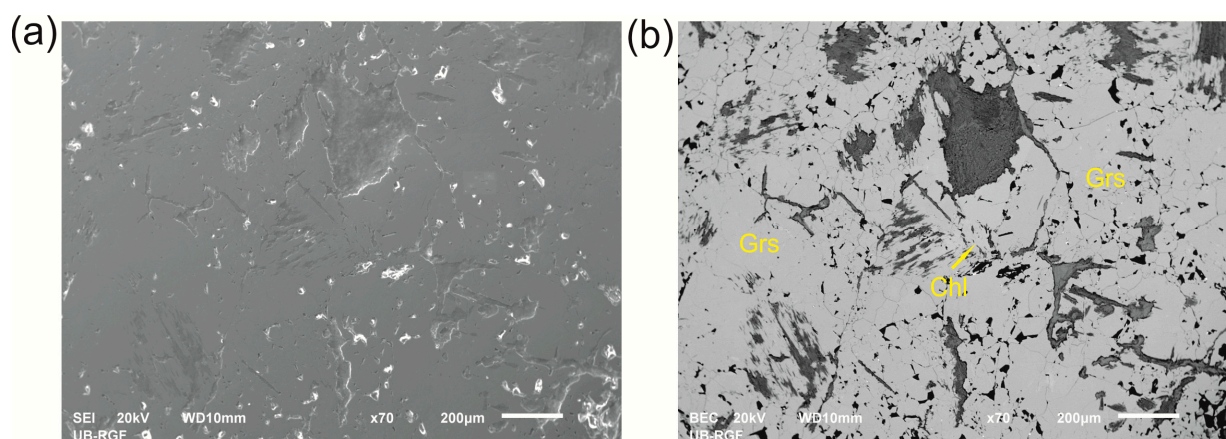


**Figure 3.** Grossular (Grs) and chlorite (Chl) appearances on (a) SEI and (b) BEC microphotographs.

The general formula of garnet is  $[8]\{X\}_3[6]\{Y\}_2[4]\{Z\}_3[4]O_{12}$ , where the eight-coordinated dodecahedral {X} site contains  $Ca^{2+}$ ,  $Mg^{2+}$ ,  $Mn^{2+}$ , or  $Fe^{2+}$  cations; the six-coordinated octahedral [Y] site contains  $Al^{3+}$ ,  $Cr^{3+}$ ,  $Fe^{3+}$ ,  $Ti^{4+}$ , or  $Zr^{4+}$  cations; and the four-coordinated tetrahedral (Z) site contains  $Si^{4+}$ ,  $Al^{3+}$ , or  $Fe^{3+}$  cations, or  $(O_4H_4)$  groups [19].

The representative spot for chemical analyses of the studied garnet are shown in Table 1. According to these chemical analyses in tetrahedral coordination (Z-cations), a minor amount of aluminum occurs along with the silicon, whereas in octahedral coordination (Y-cations), in addition to Al,  $Fe^{3+}$  and Ti are occurring. In dodecahedral coordination (X-cations), calcium and minor amounts of manganese occur, as well as  $Fe^{2+}$ . The average chemical composition shows that the examined garnet contains a major 91.1 mol. % of Grs component and 8.4 mol. % of Adr component. On the other hand, the amount of almandine (Alm; [3]) and spessartine (Sps; [3]) are minor, i.e., 0.1 and 0.4 mol. %, respectively; pyrope (Prp; [3]) and uvarovite (Uv; [3]) components were not detected.

**Table 1.** Representative chemical analyses of garnet spots (1–5). Their average values are also presented.

wt. %	1	2	3	4	5	Average
SiO <sub>2</sub>	39.53	39.06	39.11	39.10	39.60	39.28
TiO <sub>2</sub>	0.00	0.76	0.89	0.00	0.00	0.33
Al <sub>2</sub> O <sub>3</sub>	20.64	21.16	20.82	19.87	20.74	20.65
Cr <sub>2</sub> O <sub>3</sub>	0.00	0.00	0.00	0.00	0.00	0.00
FeO	2.26	1.89	1.97	3.62	2.17	2.38
MnO	0.00	0.36	0.50	0.00	0.00	0.17
MgO	0.00	0.00	0.00	0.00	0.00	0.00
CaO	37.47	36.66	36.62	37.24	37.13	37.02
Total	99.90	99.89	99.91	99.83	99.64	99.83
apfu	1	2	3	4	5	average
Si	2.986	2.955	2.962	2.966	2.999	2.974
Al <sup>IV</sup>	0.014	0.045	0.038	0.034	0.001	0.026
(Z)	3.000	3.000	3.000	3.000	3.000	3.000
Al <sup>VI</sup>	1.824	1.842	1.821	1.743	1.850	1.816
Fe <sup>3+</sup>	0.143	0.116	0.116	0.230	0.137	0.148
Ti	0.000	0.043	0.051	0.000	0.000	0.019
[Y]	1.967	2.001	1.987	1.973	1.987	1.983
Mg	0.000	0.000	0.000	0.000	0.000	0.000
Fe <sup>2+</sup>	0.000	0.004	0.009	0.000	0.000	0.003
Mn	0.000	0.023	0.032	0.000	0.000	0.011
Ca	3.033	2.972	2.972	3.027	3.013	3.003
{X}	3.033	2.999	3.013	3.027	3.013	3.017
wt. % *	1	2	3	4	5	average
Fe <sub>2</sub> O <sub>3</sub>	2.51	2.04	2.03	4.02	2.41	2.60
FeO	0.00	0.06	0.14	0.00	0.00	0.04
mol. %	1	2	3	4	5	average
Prp	0.0	0.0	0.0	0.0	0.0	0.0
Alm	0.0	0.1	0.3	0.0	0.0	0.1
Grs	92.7	91.2	90.3	88.4	93.1	91.1
Adr	7.3	8.0	8.4	11.6	6.9	8.4
Uv	0.0	0.0	0.0	0.0	0.0	0.0
Sps	0.0	0.8	1.1	0.0	0.0	0.4

\*-Recalculation of total iron into its tri- and di-valent iron was performed according to [20].

According to these results, the average chemical composition of the studied garnet could be illustrated as  $(\text{Ca}_{3.00}\text{Mn}_{0.01})_{3.01}(\text{Al}_{1.82}\text{Fe}_{0.15}\text{Ti}_{0.02})_{1.99}(\text{Si}_{2.97}\text{Al}_{0.03})_{3.00}\text{O}_{12}$ . Therefore, it appears to have somewhat more andradite (calculated together with Ti) content relative to the previous results [2]. Namely, it has a  $\text{Grs}_{91}\text{Adr}_{08}$  composition, which defines it more specifically as ferric iron containing grossular.

### 3.2. Crystal Structure Refinements

To determine what could be the true space group of the grossular garnet studied, two types of crystal models were tested using the Rietveld profile method and Fullprof program [21].

1. A mixture of two phases, with garnet as the first phase and including the various s.g.'s (such as cubic  $Ia\bar{3}d$  (N° 230), rhombohedral  $R\bar{3}c$  (N° 167) and  $R\bar{3}$  (N° 148), tetragonal  $I4_1/a$  (N° 88), orthorhombic  $Fddd$  (N° 70), monoclinic  $C2/c$  (N° 15), and triclinic  $I\bar{1}$  (N° 2)), and chlorite as the second phase.

2. A mixture of the three phases, i.e., the two garnet phases with the cubic  $Ia\bar{3}d$  s.g.'s and chlorite (third phase).

1. Crystal structure refinements were performed starting from the cubic  $Ia\bar{3}d$  s.g., which was nominally assigned for the garnet group [19,22]. The pseudo-Voigt peak shape function was assumed. In the last cycle of refinements, 116 parameters were varied: 100 parameters for the background description, 11 profile parameters (1 scale factor, 1 Eta (p-v) parameter, 1 overall temperature parameter, 3 parameters for the description of the halfwidths (U, V and W), 1 parameter for preferred orientation, 2 asymmetry parameters, 1 mixing parameter, and 1 zero point; Table S1); 1 parameter for the  $a_0$  unit cell dimension (Table S2); 1 *sof* at the octahedral [Y] site (Table S3); and 3 free oxygen ion coordinates. According to the previously detected presence of minor Alm and Sps components (Table 1), *sof* at the dodecahedral {X} site was justifiably presumed to be fully occupied with Ca, and therefore was not varied. These starting parameters and all of the studied s.g.'s were taken from [5].

An additional 47 parameters were taken and varied for chlorite in the triclinic  $C\bar{1}$  s.g. [23]: 1 scale factor, 1 mixing parameter, 6 lattice constant parameters, and 39 free ion coordinates.

Furthermore, for approximate estimation of the Al-Fe<sup>3+</sup> substitutions in the octahedral sites (Al<sub><a0></sub> and Al<sub>V0</sub>), we used available unit-cell dimensions (i.e., <a<sub>0</sub>> and volume V<sub>0</sub>; Table S2), which had been shown to be useful tools for this purpose in our previous studies [6,24,25]. All of the other calculated Al *sof*'s and selected Si-O, Y-O and Ca-O distances are listed in Table S3, whereas the final Rietveld plot is shown in Figure S1.

As is well-known, symmetry that drops from the  $Ia\bar{3}d$  s.g. to the other six space groups studied increases the number of ions in special and general positions, as well as the parameters of their coordinates, unit cell dimensions, and *sof*'s (Tables S1–S3). It should be also mentioned here that for the triclinic  $I\bar{1}$  s.g., instead of 100 parameters for the background description, 6 Chebyshev's polynomial parameters were used, and 2θ regions from 4° to 10° were also omitted. Crystal structure studies were performed without any constraints, whereas the *esd*'s values were multiplied with the SCOR factors [26]. The final Rietveld plots are shown in Figures S2–S7. Reliability factors for all of the studied space groups are presented in Table 2.

2. An additional seven parameters were taken and varied for the second garnet phase, which used the cubic  $Ia\bar{3}d$  s.g. in the mixture of three aforementioned phases: one scale factor, one mixing parameter, one lattice constant parameters, one *sof* at the octahedral [Y] site, and three free oxygen coordinates. Unfortunately, this refinement did not reach convergence; therefore, it is not presented. On the other hand, this result could be a good indicator that the studied grossular garnet does not crystallize as a mixture of two cubic phases.

For additional confirmation, the previous crystal structure refinements in all the seven various studied s.g.'s (i.e., Tables S1–S3 and Figures S1–S7) were performed with the constraints, which is suitable for the combination of the chemical composition (Table 1) and experimental data for Grs and Adr [19]. The applied constraints for the distances are as follows: <Si-O> = 1.645(5) Å, <Ca'-O> = 2.491(5) Å, and <Ca''-O> = 2.321(5) Å. In addition, by using the calculated Al<sub><a0></sub> and Al<sub>V0</sub> values of ca. 90–92% (Table S3), and Al<sub>d420</sub> = 89% (calculated on the basis of inter-planar spacing  $d_{420} = 2.654$  Å in the cubic  $Ia\bar{3}d$  s.g.), it was shown that the constraints of the Al *sof*'s should be 90%, which was most appropriate for

their mutually approximate average values. The results are presented in Tables 3 and S4–S6 and Figures S8–S14.

**Table 2.** Reliability factors for the studied space groups without constraints.

Space Group	$Ia\bar{3}d$	$R\bar{3}c$	$Fddd$	$C2/c$	$\bar{I}1$	$R\bar{3}$	$I4_1/a$
N–P+C	6388	6372	6363	6351	6365	6351	6364
$R_p$	16.2	16.2	16.3	14.8	18.7	16.1	16.0
$R_{wp}$	23.2	23.1	23.0	19.9	24.5	23.0	22.8
$R_{exp}$	8.14	8.11	8.11	8.10	8.11	8.10	8.11
Conventional $R_p$	14.9	13.8	14.2	20.2	25.1	14.2	14.0
Conventional $R_{wp}$	17.8	16.0	16.5	24.6	30.4	16.9	16.4
Conventional $R_{exp}$	6.24	5.64	5.82	10.02	10.08	5.97	5.84
Chi2	8.14	8.11	8.06	6.04	9.11	8.04	7.88
Chi2 (Bragg contr.)	8.83	8.68	8.50	6.20	9.41	8.46	8.32
DW-stat.	0.5154	0.5199	0.5239	0.6351	0.4193	0.5264	0.5430
DW-exp.	1.9744	1.9795	1.9824	1.9863	1.9818	1.9863	1.9821
GoF	2.8	2.8	2.8	2.4	3.0	2.8	2.8
Grossular $R_B$	5.63	5.01	5.29	8.13	13.7	5.08	4.90
Grossular $R_F$	1.93	1.65	1.75	3.87	7.65	1.68	1.65
Chlorite $R_B$	6.14	5.27	5.71	9.59	18.3	6.00	5.59
Chlorite $R_F$	1.95	1.56	1.68	4.23	6.97	1.79	1.61
Average $R_B$	5.72	5.06	5.37	8.39	14.91	5.22	5.01
Average $R_F$	1.94	1.64	1.74	3.93	7.47	1.70	1.64

According to a general comparative analysis of the results (Tables 2 and 3), it can be seen that monoclinic  $C2/c$  and triclinic  $\bar{I}1$  s.g.'s are showing a set of very poor reliability factors; this could preliminarily exclude them from the most probable solutions. On the other hand, the resulting reliability factors among the remained five studied s.g.'s are very good and are mutually similar. The only exceptions are the significantly higher Chi2 parameters for all of the s.g.'s studied, which were most likely induced by the preferred chlorite orientation, which is most expressive at the  $d$ -value of about 1.58 Å (i.e.,  $2\theta$  angle of about 58°; see Figures S1–S14). Accordingly, these reliability factors could not be used as the most accurate and decisive parameters for the true space group determination. Accordingly, as shown in our previous studies [5,6], there are additional and more specific criterions which can be of a great value in this case:

- (i) Taking into the account the mean  $\{X\}$  (i.e.,  $Ca^{2+}$  and  $Mn^{2+}$ ), and  $[Y]$  cation contents (i.e.,  $Al^{3+}$ ,  $Fe^{3+}$  and  $Ti^{4+}$ ) from the SEM-EDS analyses (Table 1) and using the data given by [27], the average cation sizes in  $\{X\}$  and  $[Y]$  positions were calculated to be  $\langle r_{\{x\}} \rangle = 1.119$  Å and  $\langle r_{[y]} \rangle = 0.544$  Å, respectively. The position of the grossular studied in this paper (SČ; Figure 4), clearly indicates a possibility of the  $T_{2g}$  irreducible representation, i.e., the phase transition from the cubic  $Ia\bar{3}d$  s.g., to the non-cubic  $R\bar{3}c$ ,  $Fddd$ ,  $C2/c$  and  $\bar{I}1$  s.g.'s [28];
- (ii) The calculated rhombohedral distortion angles ( $\alpha$ ) depart significantly (i.e., by more than 0.004°) from 60° (i.e., 0.036° in the  $R\bar{3}c$  s.g. and from 0.036° to 0.044° in the  $R\bar{3}$  s.g.; Tables S2 and S5), which clearly reveals the violation of the cubic symmetry [29]. Furthermore,  $\beta_0$  angles were determined to be 90.45(2)° in the triclinic  $\bar{I}1$  s.g. (Tables S2 and S5), allowing us to decisively conclude that the studied grandite is not cubic, and to assume that, actually, a structural disymmetrization occurred;

- (iii) Because there were no significant differences between Al *sof*'s and their corresponding Y–O distances over the octahedral Y sites (Table S3), the  $R\bar{3}c$  (required conditions are four different *sof*'s and Y–O distances),  $C2/c$  (required conditions are four different *sof*'s and Y–O distances) and  $\Gamma 1$  (required conditions are eight different *sof*'s and Y–O distances) s.g.'s should also be definitively excluded as viable possibilities. Therefore, only the  $I4_1/a$ ,  $R\bar{3}c$  and  $Fddd$  s.g.'s remained as plausible possibilities;

**Table 3.** Reliability factors for the studied space groups with constraints.

Space Group	$Ia\bar{3}d$	$R\bar{3}c$	$Fddd$	$C2/c$	$\Gamma 1$	$R\bar{3}$	$I4_1/a$
N–P+C	6389	6373	6364	6351	6369	6353	6365
$R_p$	16.7	16.4	16.5	16.3	19.5	16.6	16.2
$R_{wp}$	23.5	23.3	23.4	22.7	25.8	23.5	23.2
$R_{exp}$	8.13	8.12	8.11	8.10	8.11	8.10	8.11
Conventional $R_p$	15.1	14.3	15.3	20.9	27.4	14.5	14.8
Conventional $R_{wp}$	17.8	16.8	18.2	26.4	33.2	17.0	17.9
Conventional $R_{exp}$	6.16	5.87	6.32	9.43	10.42	5.85	6.28
Chi2	8.35	8.22	8.32	7.83	10.1	8.43	8.15
Chi2 (Bragg contr.)	9.06	8.80	8.76	8.02	10.5	8.90	8.61
DW-stat.	0.5041	0.5115	0.5048	0.4984	0.3805	0.5005	0.5215
DW-exp.	1.9741	1.9792	1.9821	1.9863	1.9805	1.9857	1.9818
GoF	2.9	2.8	2.8	2.8	3.1	2.9	2.8
Grossular $R_B$	6.35	5.54	6.56	10.0	16.2	6.39	5.58
Grossular $R_F$	2.23	1.86	2.19	4.04	9.36	2.06	1.89
Chlorite $R_B$	5.75	5.34	6.44	9.64	20.2	5.66	6.10
Chlorite $R_F$	1.78	1.49	1.95	3.89	8.10	1.67	1.88
Average $R_B$	6.23	5.50	6.54	9.93	17.23	6.27	5.66
Average $R_F$	2.14	1.79	2.14	4.02	9.04	1.99	1.89

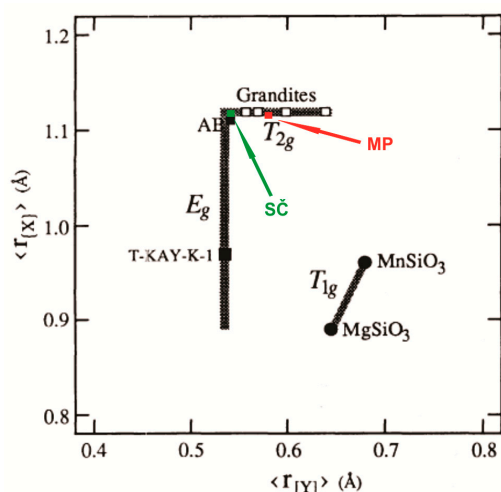


**Figure 4.** Distribution of the average cation sizes at {X} and [Y] sites of the non-cubic garnets (after [28]; black). Position of the grossular studied in this paper is marked as SČ-Suva Česma (green), whereas position of the rhombohedral ( $R\bar{3}c$  s.g.)  $Gr_{58-64}Adr_{36-41}Sp_{s2}$  grossular [6] is marked as MP-Meka Presedla (red). Inset was taken and slightly modified from [6].

- (iv) Among the later three remained solutions, the *Fddd* s.g. shows a greatest different *sof*'s of  $\Delta Al = 22(11) \%$ , whereas *I4<sub>1</sub>/a* and *R<sup>-3</sup>c* s.g.'s show *sof*'s that are equal to their *esd*'s ( $\Delta Al = 1(1) \%$  and  $\Delta Al = 12(12) \%$ , respectively). On the other hand, the resulting  $\Delta Y$ 's for the *I4<sub>1</sub>/a*, *R<sup>-3</sup>c*, and *Fddd* s.g.'s are 0.06(3) Å, 0.12(2) Å and 0.08(7) Å, respectively (Table S3). Furthermore, there is a somewhat different situation with the applied constraints (Table S6). Namely, *I4<sub>1</sub>/a*, *R<sup>-3</sup>c*, and *Fddd* s.g.'s show  $\Delta Al$ 's of 4(6) %, 22(3) %, and 14(13) %, respectively; and  $\Delta Y$ 's of 0.054(6) Å, 0.060(6) Å, and 0.075(6) Å, respectively. According to the aforementioned resulting data, there is still a considerable lack of sufficiently clear evidence and reliability of the parameters for the true space group of crystallization within these three possible solutions;
- (v) For the *Fddd*, *C2/c*, and *I*1 s.g.'s, all of the three crystallographic unit cell parameters are more or less different relative to each other, which is a required condition for these space groups (Tables S2 and S5). This fact allows us to finally exclude the *I4<sub>1</sub>/a* and *R<sup>-3</sup>c* s.g.'s as options, as well, because for the aforementioned space groups, the required conditions are that the *a*<sub>0</sub> and *b*<sub>0</sub> axes must be equal and different from the *c*<sub>0</sub> axis.

Therefore, previous results and discussion are sufficient to conclude that the studied grossular crystallized in the orthorhombic *Fddd* space group. Such characteristics align this sample further into a group that includes only a few orthorhombic garnets within the grossular-andradite solid-solution series, and the first occurrence of such a garnet in Serbia. The five previously studied orthorhombic specimens were extracted from Moravia (Czechoslovakia) and Kamaishi (Japan) [9], Hortsavinya (Spain) [15], Bazhenovskoe (Russia) [12], and Eden Mills (USA) [16]. There is also one birefringent uvarovite from Saranov (Russia) that belongs to the same orthorhombic *Fddd* space group [30]. Among these, the studied grossular has the highest content of the Grs component, and its properties are presented in more detail in Tables 4, S7 and S8, and Figures 5 and 6.

**Table 4.** Atom parameters (in Å) and calculated Al *sof*'s (at. %) for the orthorhombic *Fddd* space group (without <sup>a</sup> and with <sup>b</sup> constraints).

	Site		<i>Fddd</i> <sup>a</sup>		<i>Fddd</i> <sup>b</sup>	
			Coord.	<i>sof</i> 's	Coord.	<i>sof</i> 's
8a <sup>§</sup>	Ca1	x	0.375	0.250 (0)*	0.375	0.250 (0)
		y	0.875		0.875	
		z	0.375		0.375	
8b	Ca2	x	0.125	0.250 (0)	0.125	0.250 (0)
		y	0.625		0.625	
		z	0.125		0.125	
32h	Ca3	x	0.436(2)	1.000 (0)	0.4370(4)	1.000 (0)
		y	0.563(5)		0.5633(4)	
		z	0.251(4)		0.2533(6)	
16c	Al1	x	0.250	0.57 (6)	0.250	0.49 (6)
		y	0.000		0.000	
		z	0.250		0.250	
	Fe1	x	0.250	−0.07 (6)	0.250	0.01 (6)
		y	0.000		0.000	
		z	0.250		0.250	

Table 4. Cont.

	Site	<i>Fddd</i> <sup>a</sup>		<i>Fddd</i> <sup>b</sup>		
		Coord.	<i>sof</i> 's	Coord.	<i>sof</i> 's	
16d	Al2	x	0.250	0.46 (6)	0.250	
		y	0.500		0.500	
		z	0.250		0.250	
	Fe2	x	0.250	0.04 (6)	0.250	
		y	0.500		0.500	
		z	0.250		0.250	
16g	Si1	x	0.375	0.500 (0)	0.375	
		y	0.875		0.875	
		z	0.115(7)		0.125(1)	
32h	Si2	x	0.319(3)	1.000 (0)	0.3203(5)	
		y	0.689(6)		0.6919(6)	
		z	0.242(4)		0.2450(9)	
32h	O1	x	0.291(6)	1.000 (0)	0.2914(7)	
		y	0.74(1)		0.7540(6)	
		z	0.35(1)		0.344(1)	
32h	O2	x	0.304(7)	1.000 (0)	0.3036(6)	
		y	0.90(1)		0.902(1)	
		z	0.21(1)		0.2116(9)	
32h	O3	x	0.415(5)	1.000 (0)	0.4135(7)	
		y	0.694(9)		0.6951(7)	
		z	0.19(1)		0.204(1)	
32h	O4	x	0.154(7)	1.000 (0)	0.151(1)	
		y	0.554(8)		0.5528(6)	
		z	0.30(1)		0.2884(9)	
32h	O5	x	0.308(7)	1.000 (0)	0.3070(7)	
		y	0.60(1)		0.6010(8)	
		z	0.29(1)		0.293(1)	
32h	O6	x	0.247(7)	1.000 (0)	0.2471(6)	
		y	0.709(8)		0.7066(8)	
		z	0.16(6)		0.155(1)	
	Al1		114(11)	103 (11)	97(13)	90 (13)
	Al2		92(11)		83(13)	

§-Wyckoff positions. \*-The numbers in parentheses are the *esd*'s multiplied with SCOR [26] and refer to the last significant number.

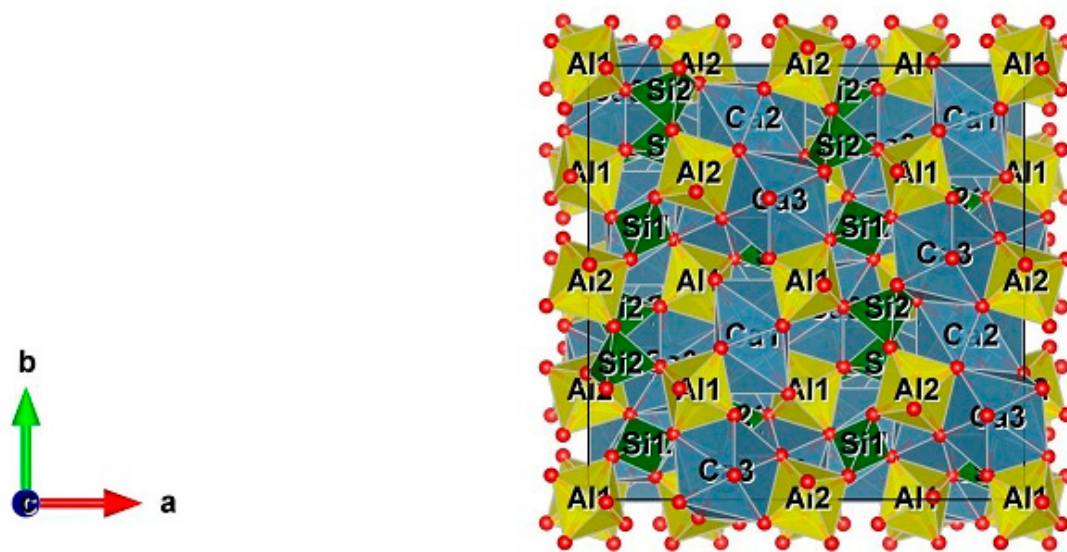


**Figure 5.** Crystal structure of the studied grossular in the  $Fddd$  space group viewed along the  $c$  axis. The  $\text{SiO}_4$  tetrahedra,  $\text{YO}_6$  octahedra, and  $\text{CaO}_8$  dodecahedra are shown with green, yellow, and blue colors, respectively. The oxygen atoms are presented with solid circles and red color. The polyhedral crystal structure was drawn using the VESTA 3 program [31].

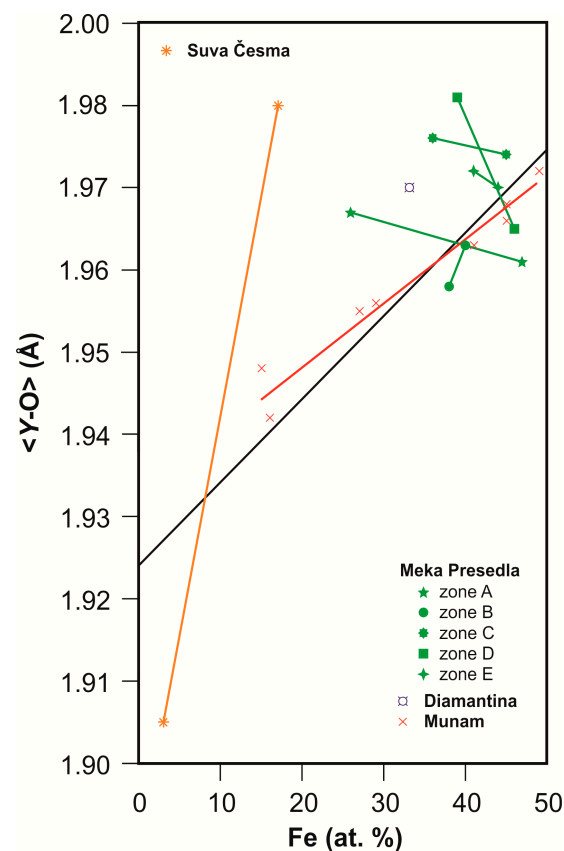


**Figure 6.** Comparison of the  $\text{Fe}^{3+}$  and  $\text{Al}^{3+}$  variations over the octahedral sites by the octahedral average  $\langle \text{Y-O} \rangle$  distances for the grossular garnets from: Suva Česma (orthorhombic  $Fddd$  s.g.; orange), Meka Presedla (rhombohedral  $R\bar{3}c$  s.g.; green), Diamantina (cubic  $Ia\bar{3}d$  s.g.; blue), and Munam (triclinic  $I\bar{1}$  s.g.; red) localities. The linear Grs-Adr join (black; after [19]) was plotted for additional comparison. Inset was taken and modified from [6].

Table S3 shows that the calculated Al *sof*'s in most of the studied space groups are more or less inconsistent with the ones expected from the chemical composition (Table 1); more specifically, the *sof*'s values are significantly higher. On the other hand, Al<sub><ao></sub> and Al<sub>V0</sub> values, which were calculated from the unit-cell dimensions (Table S3), are mostly in a very good agreement (except for the C2/c and  $I\bar{1}$  s.g.'s), showing ca. 90–92%. A similar situation was already noticed in our previous study [5,6], providing an explanation that this could be interpreted as a consequence of polyhedral distortions and/or crystal disordering because the resulting <D–O> distances are within the expected distance of 2.097 Å (see Tables 1, S3, S6 and S7).

Taking into account the distances and angles characterized without constraints (Tables S7 and S8), the results show that the grossular studied is more or less disordered and that polyhedral distortions have occurred. Namely, although they are within the *esd*'s, the distances <Si–O> and <O–O><sub>tet</sub> are somewhat shorter, whereas <Y–O>, <O–O><sub>oct</sub>, <Ca–O>, and <O–O><sub>dod</sub> are a bit longer than expected. On the other hand, the angles <O–Si–O> and <O–Y–O> are within the expected values, whereas the <O–Ca–O> angle is somewhat larger.

From the shorter <Si–O> and <O–O><sub>tet</sub> distances (Tables S3 and S7), it can be further presumed that, in the tetrahedral coordination other than silicon, a minor content (ca. 1%) of vacancies (□) could be present instead of aluminum (which could be therefore transferred into the octahedral site). It could be also speculated that, in the octahedral site, some small part of the Fe<sup>3+</sup> could be replaced by Fe<sup>2+</sup> with larger cation size [27], contributing to the aforementioned Al<sub><ao></sub> and Al<sub>V0</sub>, whereas the dodecahedral site is fully occupied with Ca<sup>2+</sup>. In that case, the average chemical composition of the studied garnet could be presented as Ca<sub>3.00</sub>(Al<sub>1.85</sub>Fe<sub>0.15</sub>Ti<sub>0.02</sub>)<sub>2.02</sub>(Si<sub>2.97</sub>□<sub>0.03</sub>)<sub>3.00</sub>O<sub>12</sub> and Grs<sub>92</sub>Adr<sub>07</sub>; which is almost identical to that previously obtained with the SEM-EDS analyses (Table 1).

Furthermore, by taking into account determined distances without any constraints between the various Si, Y, and Ca cation sites (Table S8), the most expressive distortions are within the following: (i) considerably shorter Y(2)–Si(1), Ca(2)–Si(1), and <Ca(3)–Ca(3)> distances and (ii) considerably longer <Si(1)–Si(2)>, Y(1)–Si(1), Ca(1)–Si(1), Ca(2)–Si(2), and Ca(1)–Ca(3) distances. Hence, among the studied cations within the crystal structure (Figure 5), the Si(1), Si(2), and Ca(3) cations are more or less displaced from the expected positions for the cubic *Ia*<sup>−3</sup>*d* s.g. [19], which additionally corroborates the lower symmetry. Namely, the Si(1) cation is displaced away from the Si(2), Y(1), and Ca(1) cations and towards the Y(2) and Ca(2) cations because Y(1), Y(2), Ca(1) and Ca(2) cations are in special positions with fixed coordinates (Table 4). Similarly, the Si(2) cation is displaced away from the Ca(2); whereas the Ca(3) cation is displaced away from the Ca(1), leaning towards the other Ca(3) cation.

Because there are a considerable number of distances which also deviate from the expected positions for the cubic *Ia*<sup>−3</sup>*d* s.g. [19] after applied constraints (Tables S7 and S8), the resulting orthorhombic *Fddd* s.g. should be considered as disordered.

A comparison of the Al<sup>3+</sup>–Fe<sup>3+</sup> variations over the octahedral sites by the octahedral average <Y–O> distances for the grossular garnets from Suva Česma (orthorhombic *Fddd* s.g.; this paper), Meka Presedla (rhombohedral *R*<sup>−3</sup>*c* s.g.; [6]), Diamantina (cubic *Ia*<sup>−3</sup>*d* s.g.; [32]), and Munam (triclinic *I*<sup>−1</sup> s.g.; [9]) localities is presented in Figure 6.

Considering the formation conditions of the studied grossular, it should be taken into account that the results show the transformation from the triclinic to the orthorhombic crystal structure occurring in the range of 150–350 °C [33]. On the other hand, the upper temperature limit could almost certainly be under ca. 600 °C, i.e., below the area of the rhombohedral *R*<sup>−3</sup>*c* s.g. [4–6] that has a higher symmetry.

Finally, the results show that the quantitative content is 89(8) % of grossular and 11(2) % of chlorite (Table S2), which is in good agreement with the previous macroscopic and microscopic estimations [2]. Triclinic chlorite has the following unit cell dimensions: *a*<sub>0</sub> = 5.328(3) Å, *b*<sub>0</sub> = 9.290(6) Å, *c*<sub>0</sub> = 14.286(4) Å,  $\alpha_0 = 90.95(5)^\circ$ ,  $\beta_0 = 97.08(5)^\circ$ ,  $\gamma_0 = 89.62(5)^\circ$ , and *V*<sub>0</sub> = 701.6(6) Å<sup>3</sup>. Unfortunately, there are limited opportunities for additional research

regarding the presence of chlorite in this quantity in a mixture with grossular; the XRPD patterns analysis [5,6] would be possible, mainly because of their mutually extensive overlap of their diffraction peaks (see Figures S1–S14). Namely, a close inspection of the presence and nature of the grossular reflections could be useful for checking the: (1) possible doublets and extra-broadening and (2) possible mixture of two garnet phases with the cubic  $Ia\bar{3}d$  space groups.

#### 4. Conclusions

The grossular garnet from rodingite rock from the Suva Česma locality (western Serbia) is characterized with its weak anisotropic nature and  $Gr_{91}Adr_{08}$  composition. The results further show that grossular garnet crystallized in the disordered  $Fddd$  space group, which aligned this sample further with a group of rare orthorhombic garnets within the grossular-andradite-uvarovite solid-solution series on the global scale; this sample was the first occurrence in Serbia. The results outline the temperature framework, ranging from 150 to ~600 °C.

**Supplementary Materials:** The following supporting information can be downloaded at: <https://www.mdpi.com/article/10.3390/powders2020023/s1>, Table S1. Profile parameters for the studied space groups without constraints.; Table S2. Unit cell dimensions and quantitative contents of garnet and chlorite for the studied space groups without constraints. Calculated  $4 \times c_0/a_0$  parameters and distortion angles ( $\alpha$ ) for the rhombohedral  $R\bar{3}c$  and  $R\bar{3}$  s.g.'s, and specific geometry–mathematical transformations [5,6] of the crystallographic axes within  $Ia\bar{3}d$ ,  $R\bar{3}c$ ,  $R\bar{3}$ ,  $Fddd$ ,  $C2/c$ , and  $I\bar{1}$  s.g.'s are also presented.; Table S3. Calculated Al *sof*'s (in %) and selected Si–O, Y–O, and Ca–O distances (in Å) for the studied space groups without constraints.; Table S4. Profile parameters for the studied space groups with constraints.; Table S5. Unit cell dimensions and quantitative contents of garnet and chlorite for the studied space groups with constraints. Calculated  $4 \times c_0/a_0$  parameters and distortion angles ( $\alpha$ ) for the rhombohedral  $R\bar{3}c$  and  $R\bar{3}$  s.g.'s, and specific geometry–mathematical transformations [5,6] of the crystallographic axes within  $Ia\bar{3}d$ ,  $R\bar{3}c$ ,  $R\bar{3}$ ,  $Fddd$ ,  $C2/c$ , and  $I\bar{1}$  s.g.'s, are also presented.; Table S6. Calculated Al *sof*'s (in %) and selected Si–O, Y–O, and Ca–O distances (in Å) for the studied space groups with constraints.; Table S7. Selected distances (in Å) and angles (in °) for the orthorhombic  $Fddd$  space group (without<sup>a</sup> and with<sup>b</sup> constraints).; Table S8. Selected distances among the studied cation sites (in Å) for the orthorhombic  $Fddd$  space group (without<sup>a</sup> and with<sup>b</sup> constraints).; Figure S1. Final Rietveld plot for the  $Ia\bar{3}d$  space group without constraints. Observed intensities ( $Y_{obs}$ ) were presented with red color, calculated intensities ( $Y_{calc}$ ) were presented with black color, and differences between observed and calculated intensities ( $Y_{obs}-Y_{calc}$ ) were presented with blue color. Reflection (Bragg) positions were presented with green vertical bars; upper row: garnet; lower row: chlorite.; Figure S2. Final Rietveld plot for the  $R\bar{3}c$  space group without constraints. Observed intensities ( $Y_{obs}$ ) were presented with red color, calculated intensities ( $Y_{calc}$ ) were presented with black color, and differences between observed and calculated intensities ( $Y_{obs}-Y_{calc}$ ) were presented with blue color. Reflection (Bragg) positions were presented with green vertical bars: upper row: garnet; lower row: chlorite.; Figure S3. Final Rietveld plot for the  $Fddd$  space group without constraints. Observed intensities ( $Y_{obs}$ ) were presented with red color, calculated intensities ( $Y_{calc}$ ) were presented with black color, and differences between observed and calculated intensities ( $Y_{obs}-Y_{calc}$ ) were presented with blue color. Reflection (Bragg) positions were presented with green vertical bars; upper row-garnet; lower row-chlorite.; Figure S4. Final Rietveld plot for the  $C2/c$  space group without constraints. Observed intensities ( $Y_{obs}$ ) were presented with red color, calculated intensities ( $Y_{calc}$ ) were presented with black color, and differences between observed and calculated intensities ( $Y_{obs}-Y_{calc}$ ) were presented with blue color. Reflection (Bragg) positions were presented with green vertical bars; upper row: garnet; lower row: chlorite.; Figure S5. Final Rietveld plot for the  $I\bar{1}$  space group without constraints. Observed intensities ( $Y_{obs}$ ) were presented with red color, calculated intensities ( $Y_{calc}$ ) were presented with black color, and differences between observed and calculated intensities ( $Y_{obs}-Y_{calc}$ ) were presented with blue color. Reflection (Bragg) positions were presented with green vertical bars; upper row: garnet; lower row: chlorite.; Figure S6. Final Rietveld plot for the  $R\bar{3}$  space group without constraints. Observed intensities ( $Y_{obs}$ ) were presented with red color, calculated intensities ( $Y_{calc}$ ) were presented with black color, and differences between observed and calculated intensities ( $Y_{obs}-Y_{calc}$ ) were presented

with blue color. Reflection (Bragg) positions were presented with green vertical bars; upper row: garnet; lower row: chlorite.; Figure S7. Final Rietveld plot for the  $I4_1/a$  space group without constraints. Observed intensities ( $Y_{\text{obs}}$ ) were presented with red color, calculated intensities ( $Y_{\text{calc}}$ ) were presented with black color, and differences between observed and calculated intensities ( $Y_{\text{obs}}-Y_{\text{calc}}$ ) were presented with blue color. Reflection (Bragg) positions were presented with green vertical bars; upper row: garnet; lower row: chlorite.; Figure S8. Final Rietveld plot for the  $Ia\bar{3}d$  space group with constraints. Observed intensities ( $Y_{\text{obs}}$ ) were presented with red color, calculated intensities ( $Y_{\text{calc}}$ ) were presented with black color, and differences between observed and calculated intensities ( $Y_{\text{obs}}-Y_{\text{calc}}$ ) were presented with blue color. Reflection (Bragg) positions were presented with green vertical bars; upper row: garnet; lower row: chlorite.; Figure S9. Final Rietveld plot for the  $R\bar{3}c$  space group with constraints. Observed intensities ( $Y_{\text{obs}}$ ) were presented with red color, calculated intensities ( $Y_{\text{calc}}$ ) were presented with black color, and differences between observed and calculated intensities ( $Y_{\text{obs}}-Y_{\text{calc}}$ ) were presented with blue color. Reflection (Bragg) positions were presented with green vertical bars; upper row: garnet; lower row: chlorite.; Figure S10. Final Rietveld plot for the  $Fddd$  space group with constraints. Observed intensities ( $Y_{\text{obs}}$ ) were presented with red color, calculated intensities ( $Y_{\text{calc}}$ ) were presented with black color, and differences between observed and calculated intensities ( $Y_{\text{obs}}-Y_{\text{calc}}$ ) were presented with blue color. Reflection (Bragg) positions were presented with green vertical bars; upper row: garnet; lower row: chlorite.; Figure S11. Final Rietveld plot for the  $C2/c$  space group with constraints. Observed intensities ( $Y_{\text{obs}}$ ) were presented with red color, calculated intensities ( $Y_{\text{calc}}$ ) were presented with black color, and differences between observed and calculated intensities ( $Y_{\text{obs}}-Y_{\text{calc}}$ ) were presented with blue color. Reflection (Bragg) positions were presented with green vertical bars; upper row: garnet; lower row: chlorite.; Figure S12. Final Rietveld plot for the  $I\bar{1}$  space group with constraints. Observed intensities ( $Y_{\text{obs}}$ ) were presented with red color, calculated intensities ( $Y_{\text{calc}}$ ) were presented with black color, and differences between observed and calculated intensities ( $Y_{\text{obs}}-Y_{\text{calc}}$ ) were presented with blue color. Reflection (Bragg) positions were presented with green vertical bars; upper row: garnet; lower row: chlorite.; Figure S13. Final Rietveld plot for the  $R\bar{3}$  space group with constraints. Observed intensities ( $Y_{\text{obs}}$ ) were presented with red color, calculated intensities ( $Y_{\text{calc}}$ ) were presented with black color, and differences between observed and calculated intensities ( $Y_{\text{obs}}-Y_{\text{calc}}$ ) were presented with blue color. Reflection (Bragg) positions were presented with green vertical bars; upper row: garnet; lower row: chlorite.; Figure S14. Final Rietveld plot for the  $I4_1/a$  space group with constraints. Observed intensities ( $Y_{\text{obs}}$ ) were presented with red color, calculated intensities ( $Y_{\text{calc}}$ ) were presented with black color, and differences between observed and calculated intensities ( $Y_{\text{obs}}-Y_{\text{calc}}$ ) were presented with blue color. Reflection (Bragg) positions were presented with green vertical bars; upper row: garnet; lower row: chlorite.

**Author Contributions:** P.T.: Conceptualization, writing—original draft preparation, supervision, XRPD and Rietveld experiments, methodology, validation, investigation and visualization. S.D.: microscopic investigation and writing—review and editing. S.E.: SEM-EDS experiments, and writing—review and editing. All authors discussed the manuscript. All authors have read and agreed to the published version of the manuscript.

**Funding:** This work was financially supported by the Ministry of Science, Technological Development and Innovation of the Republic of Serbia (Grant No. 451-03-47/2023-01/200026).

**Institutional Review Board Statement:** Not applicable.

**Informed Consent Statement:** Not applicable.

**Data Availability Statement:** Not applicable.

**Acknowledgments:** Authors are grateful to Darko Spahić for his useful advices and to Aleksandar Pačevski for his technical assistance.

**Conflicts of Interest:** The authors declare no conflict of interest.

## References

1. Baranin, D. Basic Geological Map of Serbia, sheet Valjevo 4, scale 1:50,000. *Geol. Surv. Serb.* **2009**, unpublished.
2. Dušanić, S.; Tančić, P.; Popović, D. First occurrence of rodingite in Central Serbia. In Proceedings of the XIX Congress of the Carpathian-Balkan Geological Association, Thessaloniki, Greece, 23–26th September 2010; Volume 39, p. 106. Available online: <https://www.geologica-balkanica.eu/journal/39/1-2/p-106> (accessed on 3 May 2023.).

3. Warr, L.N. IMA–CNMNC approved mineral symbols. *Min. Mag.* **2021**, *85*, 291–320. [[CrossRef](#)]
4. Tančić, P.; Vulić, P.; Kaindl, R.; Sartory, B.; Dimitrijević, R. Macroscopically-zoned grandite from the garnetite skarn of Meka Presedla (Kopaonik Mountain, Serbia). *Acta Geol. Sin.* **2012**, *86*, 393–406. [[CrossRef](#)]
5. Tančić, P.; Kremenović, A.; Vulić, P. Structural dissymmetrization of optically anisotropic  $\text{Grs}_{64\pm 1}\text{Adr}_{36\pm 1}\text{SpS}_2$  grandite from Meka Presedla (Kopaonik Mt., Serbia). *Powd. Diffr.* **2020**, *35*, 7–16. [[CrossRef](#)]
6. Tančić, P.; Kremenović, A. Rietveld crystal structure refinement of a natural rhombohedral grossular-andradite garnet from Serbia. *Geol. Q.* **2022**, *66*, 1639. [[CrossRef](#)]
7. Srećković-Batočanin, D.; Vasković, N.; Milutinović, S.; Ilić, V.; Nikić, Z. Composition of zonal garnets from the garnetite exo-skarn of the ore field Rogozna (Rogozna Mts, southern Serbia). In Proceedings of the XVI Serbian Geological Congress, Donji Milanovac, Serbia, 22–25th May 2014; pp. 265–268.
8. Kostić, B.; Srećković-Batočanin, D.; Filipov, P.; Tančić, P.; Sokol, K. Anisotropic grossular-andradite garnets: Evidence of two stage skarn evolution from Rudnik, Central Serbia. *Geol. Carp.* **2021**, *73*, 17–25. [[CrossRef](#)]
9. Takéuchi, Y.; Haga, N.; Umizu, S.; Sato, G. The derivative structure of silicate garnets in grandite. *Z. Krist.* **1982**, *158*, 53–99. [[CrossRef](#)]
10. Allen, F.M.; Buseck, P.R. XRD, FTIR and TEM studies of optically anisotropic grossular garnets. *Am. Miner.* **1988**, *73*, 568–584.
11. Kingma, K.J.; Downs, J.W. Crystal-structure analysis of a birefringent andradite. *Am. Miner.* **1989**, *74*, 1307–1316.
12. Frank-Kamenetskaya, O.V.; Rozhdestvenskaya, I.V.; Shtukenberg, A.G.; Bannova, I.I.; Skalkina, Y.A. Dissymmetrization of crystal structures of grossular-andradite garnets  $\text{Ca}_3(\text{Al}, \text{Fe})_2(\text{SiO}_4)_3$ . *Struct. Chem.* **2007**, *18*, 493–500. [[CrossRef](#)]
13. Kobayashi, S.; Miyawaki, R.; Momma, K.; Fujisawa, A.; Kaneda, H. Anisotropic garnet from the Yamansu ore deposit, Xinjiang, China. *J. Miner. Petrol. Sci.* **2013**, *108*, 245–254. [[CrossRef](#)]
14. Nakamura, Y.; Kuribayashi, T.; Nagase, T. Cation ordering of {110} and {211} sectors in grandite from Mali. *J. Miner. Petrol. Sci.* **2016**, *108*, 245–254. [[CrossRef](#)]
15. Gali, S. Reduction of symmetry in grandite solid solution. *Acta Geol. Hisp.* **1984**, *19*, 287–293.
16. Badar, M.A.; Hussain, S.; Niaz, S.; ur Rehman, S. Anomalous optical variations in the grossular garnet from the Eden Mills, Belvidere Mountain (Vermont, USA). *Arab J. Geosci.* **2016**, *9*, 545. [[CrossRef](#)]
17. Hirai, H.; Nakazawa, H. Visualizing low symmetry of a grandite garnet on precession photographs. *Am. Miner.* **1986**, *71*, 1210–1213.
18. Panikorovskii, T.L.; Galuskina, I.O.; Bocharov, V.N.; Shilovskikh, V.V.; Galuskin, E.V. Merohedral Mechanism Twinning Growth of Natural Cation-Ordered Tetragonal Grossular. *Crystals* **2022**, *12*, 1638. [[CrossRef](#)]
19. Novak, G.A.; Gibbs, G.V. The crystal chemistry of the silicate garnets. *Am. Miner.* **1971**, *56*, 791–825.
20. Droop, G.T.R. A general equation for estimating  $\text{Fe}^{3+}$  concentrations in ferromagnesian silicates and oxides from microprobe analyses, using stoichiometric criteria. *Min. Mag.* **1987**, *51*, 431–435. [[CrossRef](#)]
21. Rodriguez-Carvajal, J. Program Fullprof (Computer software). In Proceedings of the Abstract of 15th Conference of International Union of Crystallography, Satellite Meeting on Powder Diffraction, Toulouse, France, 16–19 July 1990; p. 127.
22. Grew, E.S.; Locock, A.J.; Mills, S.J.; Galuskina, I.O.; Galuskin, E.V.; Hålenius, U. IMA Report, Nomenclature of the garnet supergroup. *Am. Miner.* **2013**, *98*, 785–811. [[CrossRef](#)]
23. Zanazzi, P.F.; Montagnoli, M.; Nazzareni, S.; Comodi, P. Structural effects of pressure on triclinic chlorite: A single-crystal study. *Am. Miner.* **2006**, *91*, 1871–1878. [[CrossRef](#)]
24. Tančić, P.; Dimitrijević, R.; Poznanović, M.; Pačevski, A.; Sudar, S. Crystal structure and chemical composition of ludwigite from Vranovac ore deposit (Boranj Mountain, Serbia). *Acta Geol. Sin.* **2012**, *86*, 1524–1538. [[CrossRef](#)]
25. Cvetković, Ž.; Tančić, P. Mineralogical and crystallographic characteristics of bauxites from some Grebnik's (Metohija, Serbia) ore deposits. *Geol. Anal. Balk. Poluostrva* **2019**, *80*, 45–61. [[CrossRef](#)]
26. Berar, J.F.; Lelann, P. ESD's and estimated probable error obtained in Rietveld refinements with local correlations. *J. Appl. Crystallogr.* **1991**, *24*, 1–5. [[CrossRef](#)]
27. Shannon, R.D. Revised Effective Ionic Radii and Systematic Studies of Interatomic Distances in Halides and Chalcogenides. *Acta Cryst.* **1976**, *A32*, 751–767. [[CrossRef](#)]
28. Griffen, D.T.; Hatch, D.M.; Phillips, W.R.; Kulaksiz, S. Crystal chemistry and symmetry of a birefringent tetragonal pyralpite<sub>75</sub>-grandite<sub>25</sub> garnet. *Am. Miner.* **1992**, *77*, 399–406.
29. Ishizawa, N.; Inagaki, Y. A Guide to Discriminating the Rhombohedral Cell from the Face-Centred Pseudo Cubic Cell, Ceramics Research Center. *Annu. Rep.* **2008**, *8*, 35–49.
30. Wildner, M.; Andrut, M. The crystal chemistry of birefringent natural uvarovites: Part II. Single-crystal X-ray structures. *Am. Miner.* **2001**, *86*, 1231–1251. [[CrossRef](#)]
31. Momma, K.; Izumi, F. VESTA 3 for three-dimensional visualization of crystal, volumetric and morphology data. *J. Appl. Crystallogr.* **2011**, *44*, 1272–1276. [[CrossRef](#)]

32. Resende, J.A.L.C.; Fernandes, N.G. X-ray powder refinement of a natural garnet from Diamantina, Minas Gerais, Brazil. *Acta Cryst.* **2005**, *E61*, 265–267. [[CrossRef](#)]
33. Shtukenberg, A.G.; Popov, D.Y.; Punin, Y.O. Growth ordering and anomalous birefringence in ugrandite garnets. *Min. Mag.* **2005**, *69*, 537–550. [[CrossRef](#)]

**Disclaimer/Publisher’s Note:** The statements, opinions and data contained in all publications are solely those of the individual author(s) and contributor(s) and not of MDPI and/or the editor(s). MDPI and/or the editor(s) disclaim responsibility for any injury to people or property resulting from any ideas, methods, instructions or products referred to in the content.